# Bound states in inhomogeneous magnetic field in graphene: Semiclassical approach

A. Kormányos,[1] P. Rakyta,[2] L. Oroszlány,[1] and J. Cserti[2]
[1]*Department of Physics, Lancaster University, Lancaster, LA1 4YB, United Kingdom*
[2]*Department of Physics of Complex Systems, Eötvös University, H-1117 Budapest, Pázmány Péter sétány 1/A, Hungary*
(Received 16 May 2008; revised manuscript received 2 July 2008; published 28 July 2008)

We derive semiclassical quantization equations for graphene monolayer and bilayer systems where the excitations are confined by the applied inhomogeneous magnetic field. The importance of a semiclassical phase, a consequence of the spinor nature of the excitations, is pointed out. The semiclassical eigenenergies show good agreement with the results of quantum-mechanical calculations based on the Dirac equation of graphene and with numerical tight-binding calculations.

DOI: 10.1103/PhysRevB.78.045430 PACS number(s): 73.22.Dj, 03.65.Sq, 03.65.Vf

## I. INTRODUCTION

Observation of massless Dirac fermion-type excitations in recent experiments on graphene has generated huge interest both experimentally and theoretically.[1–3] For reviews on graphene, see Refs. 4–8 and a special issue in Ref. 9.

The intensive theoretical and experimental works have led to good understanding of the physical phenomena in the bulk of disorder-free graphene in homogeneous magnetic field.[10,11] Recently, the interest in inhomogeneous magnetic-field setups has also appeared. Martino *et al.*[12] have demonstrated that massless Dirac electrons can be confined by inhomogeneous magnetic field and that a magnetic quantum dot can be formed in graphene, levels of which are tunable almost at will. The so-called "snake states" known from studies[13,14] on two-dimensional electron gas (2DEG) have also attracted interest and their properties have been discussed in graphene monolayer[15,16] and in carbon nanotubes.[17,18] Furthermore, Peeters and co-workers[19] have studied the transmission through complex magnetic barrier structures.

Semiclassical methods have helped our understanding of complicated physical phenomena enormously and become a standard tool of investigation. Not only they offer a simple and easy-to-grasp classical picture but in many cases, they can also give quantitative predictions on observables. Yet the first semiclassical study on graphene systems[20] has only very recently appeared. In Ref. 20 Ullmo and Carmier derived an expression for the semiclassical Green's function in graphene and studied the "Berry-like" phase which appears in the semiclassical theory. The importance of Berry-like and "non-Berry-like" phases in the asymptotic theory of coupled partial differential equations and their roles in semiclassical quantization were previously discussed in Refs. 21–24.

In this work we study a graphene nanoribbon[25] in a nonuniform magnetic field[12,15,16] as shown in Figs. 1(a) and 1(b) and a circular magnetic dot in graphene monolayer[12] [see Fig. 1(c)]. We assume that the applied perpendicular magnetic field of magnitude $|B_z|$ changes to step-function-like manner at the interfaces of the magnetic and nonmagnetic regions and that it is strong enough so that the magnetic length $l_B=\sqrt{\hbar/e|B_z|}$ is much smaller than the characteristic spatial dimension of the graphene sample. We show that in this case the semiclassical quantization can predict and can help understand the main features of the quantum spectra at the **K** point[4–8] of graphene monolayer and bilayer.

The article is organized in the following way. First, in Sec. II we give a brief overview of the exact quantum-mechanical treatment of graphene monolayer and bilayer. We also discuss some of the technical details of the quantum calculation regarding the system shown in Fig. 1. Next, in Sec. III we introduce our semiclassical formalism and whenever possible, we give a unified description for graphene monolayer and bilayer. In Sec. IV we present the results of the semiclassical quantization for graphene nanoribbons in inhomogeneous magnetic field and compare it with tight-binding (TB) and exact quantum calculations. In Sec. V we apply the semiclassical formalism to a magnetic dot in graphene monolayer. Finally, in Sec. VI we arrive to our conclusions.

## II. MONOLAYER AND BILAYER GRAPHENE: QUANTUM-MECHANICAL TREATMENT

In the simplest approximation the Dirac Hamiltonian describing the low-energy excitations at the **K** point of the

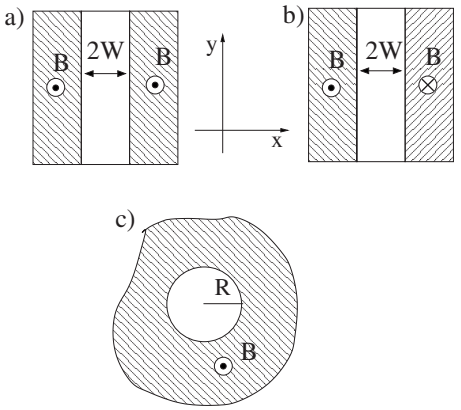


FIG. 1. In (a) and (b) the applied perpendicular magnetic field **B** is zero in the center region of width $2W$. In the case of (a), in the left and right regions the magnetic fields point in the same directions, while in the case of (b), in the opposite directions. The magnitude $B$ of the magnetic field is the same in both left and right regions. In the case of Fig. 1(c) a circular nonmagnetic region of radius $R$ is considered in graphene monolayer, whereas outside this region there is perpendicularly applied magnetic field of magnitude $B$.

 

Brillouin zone in monolayer (bilayer) graphene reads

$$\hat{H}_\beta = g_\beta \begin{pmatrix} 0 & (\hat{\pi}_x - i\hat{\pi}_y)^\beta \\ (\pi_x + i\hat{\pi}_y)^\beta & 0 \end{pmatrix}. \quad (1)$$

Here $\beta=1(2)$ for monolayer (bilayer), and $g_1=v_F=\sqrt{3}/2at_1/\hbar$ is given by the hopping parameter $t_1$ between the nearest neighbors in monolayer graphene ($a=0.246$ nm is the lattice constant in the honeycomb lattice). Moreover, $g_2=-1/2m^*$ and the mass term is given by $m^*=t_2/2(g_1)^2$ with $t_2$ being the interlayer hopping between $\tilde{A}-B$ sites of bilayer.[11] The operators $(\hat{\pi}_x,\hat{\pi}_y)$ are defined by $\hat{\pi}=(\hat{\pi}_x,\hat{\pi}_y)=\hat{\mathbf{p}}+e\mathbf{A}$, where $\hat{\mathbf{p}}=\frac{\hbar}{i}\frac{\partial}{\partial \mathbf{r}}$ is the canonical momentum operator and the vector potential $\mathbf{A}$ is related to the magnetic field through $\mathbf{B}=\text{rot}\ \mathbf{A}$. Due to the chiral symmetry $\sigma_z\hat{H}_\beta\sigma_z=-\hat{H}_\beta$, where $\sigma_z$ is a Pauli matrix, it is enough to consider the positive eigenvalues of the Hamiltonian $\hat{H}_\beta$.

In Sec. IV we study a graphene nanoribbon of width $L \gg l_B$ [see Figs. 1(a) and 1(b)]. In the central region $|x|<W$ the magnetic field is zero, while for $|x|\geq W$ a nonzero perpendicular magnetic field is applied. We assume a step-function-like change in the magnetic field at $x=W$ and use the vector potential $\mathbf{A}(\mathbf{r})=(0,A_y(x),0)^T$ to preserve the translation invariance in the $y$ direction. Other details of the quantum calculation can be found in Refs. 12, 15, and 16.

The magnetic dot system is shown in Fig. 1(c). It consists of a graphene monolayer in homogeneous perpendicular magnetic field with a circular enclosure where the magnetic field is zero. The circular symmetry of the setup suggests that one should choose the vector potential in the symmetric gauge,

$$\mathbf{A}(\mathbf{r}) = \begin{cases} 0 & r < R, \\ \dfrac{B_z(r^2-R^2)}{2r}\begin{pmatrix} -\sin\varphi \\ \cos\varphi \\ 0 \end{pmatrix} & r \geq R, \end{cases} \quad (2)$$

where $\mathbf{r}=(r\cos\varphi, r\sin\varphi)$ is in polar coordinates. One can show that with this choice the Schrödinger equation $\hat{H}_\beta\Psi_\beta=E\Psi_\beta$ becomes separable in $r$ and $\varphi$. In the case of graphene monolayer, requiring the wave function to be normalizable and continuous at $r=R$ leads to a secular equation, solutions of which are the quantum eigenenergies [see Eq. (21) in Ref. 16].

## III. SEMICLASSICAL FORMALISM FOR GRAPHENE

We now give a brief account of our semiclassical formalism. Our discussion goes along the lines of the Refs. 20, 23, and 24 from where we have also borrowed some of the notations.

We seek the solutions of the Schrödinger equation $\hat{H}_\beta\Psi_\beta=E\Psi_\beta$ in the following form:[24]

$$\Psi_\beta(\mathbf{r}) = \sum_{k\geq 0}\left(\frac{\hbar}{i}\right)^k \mathbf{a}_k^\beta(\mathbf{r}) e^{\frac{i}{\hbar}S_\beta(\mathbf{r})}, \quad (3)$$

where $\mathbf{a}_k^\beta(\mathbf{r})$ are spinors and $S_\beta(\mathbf{r})$ is the classical action. Performing the unitary transformations $\Psi_\beta \to e^{-\frac{i}{\hbar}S_\beta(\mathbf{r})}\Psi_\beta$ and $\hat{H}_\beta \to e^{-\frac{i}{\hbar}S_\beta(\mathbf{r})}\hat{H}_\beta e^{\frac{i}{\hbar}S_\beta(\mathbf{r})}$, the Schrödinger equation can be rewritten as

$$\begin{pmatrix} -E & g_\beta(\hat{\Pi}_x - i\hat{\Pi}_y)^\beta \\ g_\beta(\hat{\Pi}_x + i\hat{\Pi}_y)^\beta & -E \end{pmatrix}\left(\mathbf{a}_0^\beta(\mathbf{r}) + \frac{\hbar}{i}\mathbf{a}_1^\beta(\mathbf{r}) + \ldots\right) = 0. \quad (4)$$

Here $\hat{\Pi}_x=\hat{p}_x+\Pi_x^0$, where $\Pi_x^0=p_x+eA_x(\mathbf{r})$, $p_x=\frac{\partial S_\beta(\mathbf{r})}{\partial x}$, and similarly for $\hat{\Pi}_y$. The WKB strategy[26] is to satisfy Eq. (4) separately order by order in $\hbar$.

At $\mathcal{O}(\hbar^0)$ order we obtain

$$\begin{pmatrix} -E & g_\beta(\Pi_x^0 - i\Pi_y^0)^\beta \\ g_\beta(\Pi_x^0 + i\Pi_y^0)^\beta & -E \end{pmatrix}\mathbf{a}_0^\beta(\mathbf{r}) = 0. \quad (5)$$

This classical Hamiltonian can be diagonalized with eigenvalues

$$\mathcal{H}_\beta^\pm(\mathbf{p},\mathbf{r}) = \pm g_\beta\{[\Pi_x^0(\mathbf{r})]^2 + [\Pi_y^0(\mathbf{r})]^2\}^{\beta/2} \quad (6)$$

and eigenvectors $V_\beta^\pm(\mathbf{p},\mathbf{r})$. What we have found is that the $\mathcal{O}(\hbar^0)$ order equation is in fact equivalent to a pair of classical Hamilton-Jacobi equations,

$$E - \mathcal{H}_\beta^\pm\left(\frac{\partial S_\beta^\pm(\mathbf{r})}{\partial \mathbf{r}}, \mathbf{r}\right) = 0. \quad (7)$$

The solution of Eq. (7) when it exists can be found, e.g., by the method of characteristics.[20]

For $E\neq 0$ the eigenvectors of the classical Hamiltonian given in Eq. (5) are

$$V_\beta^\pm = \frac{1}{\sqrt{2}}\begin{pmatrix} \pm(-1)^{\beta-1}e^{-i\beta\phi} \\ 1 \end{pmatrix} \quad (8)$$

(here $\phi$ is the phase of $\Pi_x^0 - i\Pi_y^0$); but the eigenspinor $\mathbf{a}_0^{\beta,\pm}$ can be more generally written as $\mathbf{a}_0^{\beta,\pm}=\mathcal{A}_\beta^\pm(\mathbf{r})e^{i\gamma_\beta^\pm(\mathbf{r})}V_\beta^\pm$ where $\mathcal{A}_\beta^\pm(\mathbf{r})$ is a real amplitude and $\gamma_\beta^\pm(\mathbf{r})$ is a phase. Equations for $\mathcal{A}_\beta^\pm(\mathbf{r})$ and $\gamma_\beta^\pm(\mathbf{r})$ can be obtained from the $\mathcal{O}(\hbar^1)$ order of Eq. (4). One can show that the $\mathcal{O}(\hbar^1)$-order equation can be written in the following form:[20,23,24]

$$(\mathbf{a}_0^{\beta,\pm})^\dagger \hat{M}_\beta \mathbf{a}_0^{\beta,\pm} = 0. \quad (9)$$

Using the notation $\boldsymbol{\sigma}=(\sigma_x,\sigma_y)$ with $\sigma_{x,y,z}$ being the Pauli matrices, the operator $\hat{M}_1$ for graphene monolayer is $\hat{M}_1=\boldsymbol{\sigma}\hat{\mathbf{p}}$, while for bilayer it reads $\hat{M}_2=\hat{m}+\hat{m}^\dagger$ where $\hat{m}=\boldsymbol{\sigma}\hat{\mathbf{p}}(\Pi_x^0+i\sigma_z\Pi_y^0)$.

The imaginary part of Eq. (9) expresses the conservation of probability since it can be cast into the form of a continuity equation $\text{div}\ \mathbf{j}_\beta^\pm=0$. Here $\mathbf{j}_\beta^\pm=\text{Im}\langle\Psi_\beta^{s,\pm}|\hat{\mathbf{v}}_\beta|\Psi_\beta^{s,\pm}\rangle$ is the probability current carried by the semiclassical wave function $\Psi_\beta^{s,\pm}=\mathbf{a}_0^{\beta,\pm}e^{\frac{i}{\hbar}S_\beta^\pm}$ ($\hat{\mathbf{v}}_\beta=\frac{i}{\hbar}[\hat{H}_\beta,\mathbf{r}]$ is the velocity operator). Similarly to the case of quantum systems described by scalar Schrödinger equation,[26] this continuity equation determines $\mathcal{A}_\beta^\pm(\mathbf{r})$.

The real part of Eq. (9) allows calculating the phase $\gamma_\beta^\pm(\mathbf{r})$. The equation determining $\gamma_\beta^\pm(\mathbf{r})$ reads

$$\frac{d\gamma_\beta^\pm(\mathbf{r})}{dt} = c_\beta^\pm \frac{\beta}{2}\left[\frac{\partial \Pi_y^0(\mathbf{r})}{\partial x} - \frac{\partial \Pi_x^0(\mathbf{r})}{\partial y}\right] = c_\beta^\pm \frac{\beta}{2} eB_z(\mathbf{r}), \quad (10)$$

where $c_1^\pm = v_F^2/E$, $c_2^\pm = \pm 1/m^*$, and we denote by $B_z(\mathbf{r})$ the component of the applied magnetic field that is perpendicular to the graphene sheet. The second equality in Eq. (10) follows from $\frac{\partial^2 S_\beta(\mathbf{r})}{\partial x \partial y} = \frac{\partial^2 S_\beta(\mathbf{r})}{\partial y \partial x}$.

The Hamiltonian given in Eq. (1) yields a gapless spectrum for bilayer graphene. Theoretical and experimental studies of bilayer graphene[11,27] have shown that an electron-density-dependent gap can exist between the otherwise degenerate valence and conductance bands (described by $\mathcal{H}_2^-$ and $\mathcal{H}_2^+$, respectively, in our semiclassical formalism). Assuming that the gap is spatially constant, one can take it into account by considering the Hamiltonian $\hat{H}_{2,\Delta} = \hat{H}_2 + (\Delta/2)\sigma_z$ (Ref. 11). The new term $(\Delta/2)\sigma_z$ affects only the $\mathcal{O}(\hbar^0)$ calculations, while the operator $\hat{M}_2$ in Eq. (9) remains the same. Consequently, Eq. (6) is modified to

$$\mathcal{H}_2^\pm(\mathbf{p},\mathbf{r}) = \pm \frac{1}{2m^*}\sqrt{[(\Pi_x^0)^2 + (\Pi_y^0)^2]^2 + \tilde{\Delta}^2}, \quad (11)$$

where $\tilde{\Delta} = \Delta/m^*$ and the right-hand side of Eq. (10) for $\beta = 2$ is multiplied by $\eta = \sqrt{1 - \frac{\Delta^2}{4E^2}}$.

It was shown in Refs. 21, 23, and 24 that for $N$-dimensional integrable systems where the particles have an internal, e.g., spin or electron-hole degree of freedom, one can derive a generalization of the Einstein-Brillouin-Keller (EBK) (Ref. 26) quantization of scalar systems. In general, the quantization conditions read

$$\frac{1}{\hbar}\oint_{\Gamma_j} \mathbf{p}d\mathbf{r} + \alpha_j = 2\pi\left(n_j + \frac{\mu_j}{4}\right). \quad (12)$$

Here $\Gamma_j$, $j = 1 \ldots N$ are the irreducible loops on the $N$-torus in the phase space, $n_j$s are positive integers, $\mu_j$s are the Maslov indices[26] counting the number of caustic points along $\Gamma_j$, and finally $\alpha_j$s measures the change in the phase of the spinor part of the wave function as the system goes around a loop $\Gamma_j$. The systems we are considering (see Fig. 1) are more simple in a way that the Schrödinger equation is separable if the vector potential $\mathbf{A}(\mathbf{r})$ is chosen in an appropriate gauge, which takes into account the symmetry of the setup [i.e., translational symmetry in the case of Figs. 1(a) and 1(b) and rotational in the case of Fig. 1(c)]. The magnetic field $B_z$ in Eq. (10) will depend on only one of the (generalized) coordinates. Let us denote this coordinate by $x_1$, the conjugate momentum by $p_1$, and the other coordinate (conjugate momentum) by $x_2$ ($p_2$). It turns out that due to the symmetry of the system, $\gamma(\mathbf{r})$ will also depend only on $x_1$ (Ref. 28). Therefore one of the two quantization conditions, involving the coordinate $x_2$ and the conjugate momentum $p_2$, is exactly the same as it would be for a scalar wave function [this corresponds to $\alpha_2 = 0$ in Eq. (12)]. In the quantization condition involving $p_1$ and $x_1$, however, the phase $\alpha_1$ is in general not zero but is determined by Eq. (10),

$$\alpha_1 = \gamma_\beta^\pm = c_\beta^\pm \frac{\beta}{2}\oint B_z(x_1(t))dt. \quad (13)$$

For systems with piecewise constant magnetic-field profiles such as those shown in Fig. 1, the calculation of $\gamma_\beta^\pm$ simplifies to $\gamma_\beta^\pm = c_\beta^\pm \frac{\beta}{2}\Sigma_l B_{z,l} T_l$. Here $T_l$ is the time that the particle spends during one full period of its classical motion in the $l$th region where the strength of the perpendicular component of the magnetic field is given by $B_{z,l}$. In the semiclassical picture $\gamma(\mathbf{r})$ changes only when the particle, during the course of its classical motion, passes through nonzero magnetic-field regions; and this phase change in the wave function needs to be taken into account in the semiclassical quantization.

## IV. BOUND STATES IN GRAPHENE NANORIBBONS

We now apply the presented semiclassical formalism to determine the energy of the bound states in inhomogeneous magnetic-field setups in graphene nanoribbons [see Figs. 1(a) and 1(b)]. Throughout the rest of the paper we will only consider $\mathcal{H}_\beta^+$ corresponding to positive energies; $\mathcal{H}_\beta^-$ would describe negative energies. These, however, do not need to be considered separately due to the chiral symmetry of the Hamiltonian as explained in Sec. II.

Using the Landau gauge $\mathbf{A} = (0, A_y(x), 0)^T$ the translation invariance of the system in the $y$ direction is preserved and, therefore, the solution of the Hamilton-Jacobi equation Eq. (7) can be sought as $S_\beta(\mathbf{r}) = S_\beta(x) + p_y y$, where $p_y = \text{const}$. Since the classical motion in the $y$ direction is not bounded, $p_y = \hbar k_y$ is not quantized; it appears as a continuous parameter in our calculations. In contrast, the motion in the $x$ direction is bounded due to the $x$-dependent magnetic field $B_z(x)$. Therefore the quantization condition reads

$$\frac{1}{\hbar}\oint p_\beta(x)dx + \gamma_\beta = 2\pi(n + 1/2). \quad (14)$$

(Note that the Maslov index is $\mu = 2$.) It is useful to introduce at this point the following dimensionless parameters: the width of the nonmagnetic region $\tilde{w} = W/l_B$ and the guiding center coordinate $\tilde{X} = k_y l_B$, both in units of $l_B$ (which is defined in Sec. II). Throughout this paper we will use $\tilde{w} = 2.2$.

We start our discussion with the magnetic waveguide configuration shown in Fig. 1(a) in graphene monolayer. Introducing the dimensionless energy $\tilde{E}_{ml} = El_B/\hbar v_F$, one finds that for $|\tilde{X}| < \tilde{E}_{ml}$ there is one turning point in each of the left and right magnetic regions. A simple calculation gives $\gamma_1 = \pi$ and writing out explicitly the result of the action integral from Eq. (14), it follows that

$$4K_{ml}\tilde{w} + \pi\tilde{E}_{ml}^2 = 2n\pi, \quad n = 1,2, \ldots. \quad (15)$$

Here we have introduced the dimensionless wave number $K_{ml} = \sqrt{\tilde{E}_{ml}^2 - \tilde{X}^2}$ and note that the phase change in the wave function due to $\gamma(x)$ cancelled the phase contribution coming from the Maslov index. Furthermore, if $\tilde{X} > \tilde{E}_{ml}$ ($\tilde{X} < -\tilde{E}_{ml}$) there are two turning points in the left (right) magnetic region. One finds that also for this case $\gamma_1 = \pi$, which again cancels the contribution from the Maslov index; thus, for $|\tilde{X}| > \tilde{E}_{ml}$ the semiclassical quantization yields

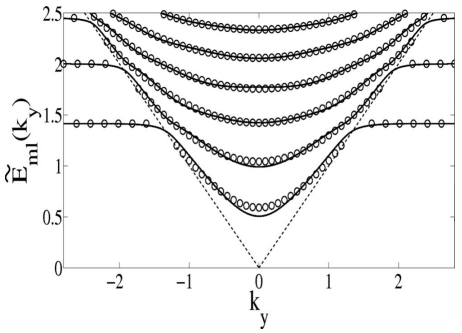


FIG. 2. Results of exact quantum calculations (solid lines) and the semiclassical approximation given by Eqs. (15) and (16) (circles) as a function of $k_y$ (in units of $l_B$) for graphene monolayer. The dashed lines indicate $|\tilde{X}|=\tilde{E}_{ml}$ (see text).

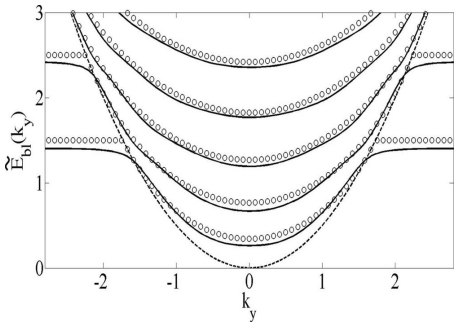


FIG. 3. Results of exact quantum calculations (solid lines) and the semiclassical approximation given by Eqs. (17) and (18) (circles) as a function of $k_y$ (in units of $l_B$) for graphene bilayer. The dashed lines indicate $\tilde{X}^2/2=\tilde{E}_{bl}$ (see text).

$$\tilde{E}_n = \sqrt{2n}, \quad n = 1, \quad 2, \quad \ldots, \tag{16}$$

i.e., the energies are independent of $\tilde{X}$ (and hence of $k_y$). This is the same as the exact quantum and the semiclassical[20] results for the relativistic Landau levels (LLs) in *homogeneous* magnetic field. [From the exact quantum calculations[16] it is known that a zero-energy state also exists in this system. Formally, from Eq. (16) one can obtain a zero-energy state by assuming that $n=0$ is admissible. However, Eq. (8) and hence Eq. (10) are only valid for $E\neq 0$. Therefore we exclude $n=0$.]

Comparison of the semiclassical eigenvalues with the results of exact quantum calculations is shown in Fig. 2. (For details of the quantum calculation see, e.g., Ref. 16.)

The agreement between the quantum and semiclassical calculations is in general very good, especially for higher energies. For lower energies and $|\tilde{X}| \gg \tilde{E}_{ml}$, one can observe quantum states which are almost dispersionless and their energies are very close to the nonzero-energy LLs in graphene monolayer. Semiclassically, these states are described by Eq. (16). Although the zero-energy state of the spectrum[16] cannot be accounted for by our semiclassics, an expression for the gap between the zero- and the first nonzero-energy states can be easily obtained by putting $n=1$ and $\tilde{X}=0$ in Eq. (15), and it gives a rather accurate prediction as can be seen in Fig. 2. The presented semiclassical method cannot describe those quantum states that correspond to $|\tilde{X}| \approx \tilde{E}_{ml}$ (see the dashed line in Fig. 2), i.e., when one of the turning points is in the area of rapid spatial variation of the magnetic field.

For comparison, we have also calculated the quantization condition for graphene bilayer using the classical Hamiltonian given in Eq. (11) and the general quantization condition shown in Eq. (14). For $\tilde{E}_{bl} > \tilde{X}^2/2$, where $\tilde{E}_{bl}=\frac{E\eta}{\hbar\omega_c}$ and $\omega_c=\frac{|eB|}{m}$ being the cyclotron frequency, it reads

$$2K_{bl}\tilde{w} + \pi\tilde{E}_{bl} = \pi\left(n - \frac{1}{2}\right), \quad n = 2,3, \quad \ldots. \tag{17}$$

Here $K_{bl}=\sqrt{2\tilde{E}_{bl}-\tilde{X}^2}$ and we have taken into account that in this case, $\gamma_2=2\pi$. For $\eta=1$ [where $\eta$ has been defined after Eq. (11)] this result is very similar to what one would obtain for a 2DEG—the only difference being that for 2DEG, one would have $+1/2$ on the right-hand side of Eq. (17). This similarity is a consequence of having a parabolic dispersion relation $E(\mathbf{k})$ close to the Fermi energy in both a 2DEG and graphene bilayer systems. We let the integer quantum number $n$ to run from $n=2$ in Eq. (17) for the following considerations: from Ref. 20 we know that in a more simple case of homogeneous magnetic field, the fourfold-degenerate[29] LL of the quantum calculations[11] at $\tilde{E}_{bl}=0$ (corresponding to $n=0$ and 1) cannot be correctly described semiclassically; but for LLs having $\tilde{E}_{bl}>0$ the agreement between the semiclassical and quantum results is qualitatively very good. Similarly, we expect that in our case the semiclassical approximation should only work for $n\geq 2$. We have found that this is indeed the case (see Fig. 3) where the solid lines show the bands obtained by TB calculations[30] and the circles are calculated using Eq. (17) for $n\geq 2$ (we have taken $\eta=1$). The $\tilde{E}_{bl}>0$ energy bands for $\tilde{E}_{bl}>\tilde{X}^2/2$ are remarkably well described by Eq. (17) (note however that like in the homogeneous magnetic-field case, there is a fourfold-degenerate state at $\tilde{E}_{bl}=0$). For $\tilde{E}_{bl}<\tilde{X}^2/2$ the bands of TB calculations again become almost dispersionless and level off very close to the LLs of bilayer graphene in homogeneous field.[11] The semiclassical expression for the energy levels in this regime of $\tilde{X}$ is

$$\tilde{E}_{bl} = (n - 1/2), \quad n = 2,3, \quad \ldots, \tag{18}$$

which is again a good approximation of the quantum result. Our semiclassics cannot correctly account for states having $\tilde{X}^2/2 \approx \tilde{E}_{bl}$, i.e., when one of the turning points is in rapidly varying magnetic-field region.

We now turn to the semiclassical study of the system depicted in Fig. 1(b) where the magnetic field is reversed in one of the regions. It was shown in Refs. 15 and 16 that peculiar type of current carrying quantum states called snake states exist close to the **K** point of graphene for this magnetic-field configuration. These states can also be described by the Dirac Hamiltonian and are therefore amenable to semiclassical treatment.

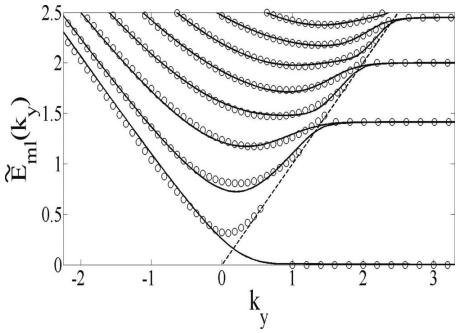


FIG. 4. Results of exact quantum calculations (solid lines) and the semiclassical approximation given by Eq. (19) (circles) as a function of $k_y$ (in units of $l_B$) for graphene monolayer. The dashed line indicates $\tilde{X}=\tilde{E}_{ml}$ (see text).

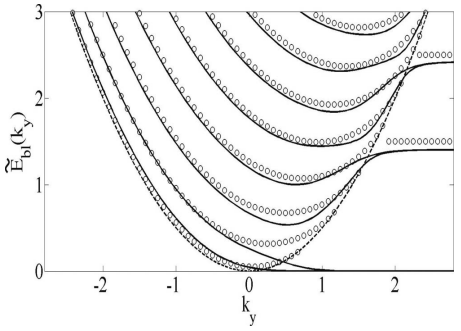


FIG. 5. Results of TB calculations (solid lines) and a semiclassical approximation (circles) for graphene bilayer as a function of $k_y$ (in units of $l_B$). The semiclassical approximation can be obtained from Eq. (19) by a transformation described in the main text. The dashed line indicates $\tilde{X}^2/2=\tilde{E}_{bl}$ (see text).

We start the discussion with the graphene monolayer case. There are no turning points and hence no states if $-\tilde{X}>\tilde{E}_{ml}$. For $|\tilde{X}|<\tilde{E}_{ml}$ there is one turning point in each of the nonzero magnetic-field regions. In contrast to the symmetric magnetic-field configuration [Fig. 1(a)], we find that for one full period of motion $\gamma_1=0$, the contributions of the two magnetic-field regions—pointing in the opposite direction—cancel. Using Eq. (14) the quantization condition is

$$K_{ml}(2\tilde{w}+\tilde{X})+\tilde{E}_{ml}^2\left[\arcsin\left(\frac{\tilde{X}}{\tilde{E}_{ml}}\right)+\frac{\pi}{2}\right]=\pi(n+1/2),$$

$$n=0,1,2,\ \ldots \tag{19}$$

Note that unlike the case of Eq. (15), here a solution for $n=0$ also exists. Moreover, for $\tilde{X}>\tilde{E}_{ml}$ there are two turning points both in the left (we denote them by $x_1^L$ and $x_2^L$) and in the right (denoted by $x_1^R$ and $x_2^R$) magnetic regions. The quantization using $x_1^L$ and $x_2^L$ leads to the same result as in Eq. (16), i.e., $\tilde{E}_{n,L}=\sqrt{2n}$, while using $x_1^R$ and $x_2^R$ gives the sequence $\tilde{E}_{n,R}=\sqrt{2(n+1)}$. The difference between $\tilde{E}_{n,L}$ and $\tilde{E}_{n,R}$ is due to the fact that the sign of the phase contribution from $\gamma(x)$ depends on the direction of the magnetic field, i.e., it is $+\pi$ when $x_1^L$ and $x_2^L$ are used in the calculations and $-\pi$ when $x_1^R$ and $x_2^R$ are used [see Eq. (10)]. From these considerations it follows that if $n=0,1,2,\ \ldots$ as we assumed in Eq. (19), the two sequences $\tilde{E}_{n,L}$ and $\tilde{E}_{n,R}$ give rise to twofold-degenerate dispersionless states at $\tilde{E}_{ml}=\sqrt{2},\sqrt{4},\sqrt{6}\ldots$ and a nondegenerate one at $\tilde{E}_{ml}=0$. We have to exclude, however, the $\tilde{E}_{ml}=0$ solution [see the discussion below Eq. (16)]. The degeneracy of the dispersionless part of the spectrum can also be understood in the following way. One can easily show that for this magnetic field profile the effective potential in the Hamiltonian $\mathcal{H}_1^+$ given by Eq. (6) has a "Mexican hat" shape for $\tilde{X}>0$ with two symmetric minima, and the energy barrier between these two minima is exactly $\tilde{X}$. Hence, if $\tilde{E}_{ml}>\tilde{X}>0$, i.e., when the particle's energy is larger then the energy barrier, it is confined by an effectively single well potential; but for $\tilde{X}\gg\tilde{E}_{ml}$ there is a degeneracy due to the fact that the Dirac particles are localized around one or the other minimum.

The results of quantum and of semiclassical calculations are shown in Fig. 4. (For details of the quantum calculation see, e.g., Ref. 15.) As one can see the agreement is again very good for $\tilde{E}_{ml}\gtrsim 0.4$ except when $\tilde{X}\approx\tilde{E}_{ml}$ [see the discussion above Eq. (17)]. The twofold-degenerate dispersionless quantum states can be clearly seen for $\tilde{X}\gg\tilde{E}_{ml}$. However, when $\tilde{X}\gtrsim\tilde{E}_{ml}$ the tunneling between the states localized around the minima of the above explained effective potential removes the degeneracy and produces the small splittings of the states, which can also be observed. States having energies $0<\tilde{E}_{ml}\lesssim 0.25$ cannot be described by our semiclassics and note that in the lowest-energy band corresponding to $n=0$ in Eq. (19), nonphysical solutions also appear along with the genuine ones for $0.25\lesssim\tilde{E}_{ml}\lesssim 0.4$. This clearly indicates the limits of applicability of our approach, i.e., it does not work for energies close to the Dirac point.

We end our discussion of the bound states in monolayer and bilayer graphene nanoribbons with the bilayer system corresponding to the previous monolayer example, e.g., for the magnetic-field setup of Fig. 1(b). For $-\tilde{X}>\sqrt{2\tilde{E}_{bl}}$ there are no turning points and hence no states. The quantization condition for $\tilde{X}^2/2<\tilde{E}_{bl}$ can simply be obtained from Eq. (19) by changing $\tilde{E}_{ml}\to\sqrt{2\tilde{E}_{bl}}$ and $K_{ml}\to K_{bl}$ [$K_{bl}$ is defined after Eq. (17)]. Finally, for $\tilde{X}^2/2>\tilde{E}_{bl}$ our semiclassics predicts a sequence of doubly degenerate dispersionless energy levels at $\tilde{E}_{bl}=(n-1/2)$, $n=2,3,\ \ldots$, in a similar fashion as in the monolayer case. As one can see in Fig. 5 for $\tilde{E}_{bl}\gtrsim 0.8$, the semiclassical approximation captures all the main features of the TB calculations quite well, apart from the region where $\tilde{X}^2/2\approx\tilde{E}_{bl}$ for $\tilde{X}>0$ [see the discussion below Eq. (18)]. Dispersive states corresponding to $n=0$ and 1 can also be described semiclassically if $\tilde{E}_{bl}\gtrsim 0.8$ [see the lowest two bands in Fig. 5], but for smaller energies nonphysical solutions along with the genuine ones do appear and for $\tilde{E}_{bl}\lesssim 0.1$ (i.e., very close to the Dirac point) no quantum states

can be described with the presented semiclassical approach.

## V. BOUND STATES OF A MAGNETIC QUANTUM DOT

Our last example is the magnetic dot in graphene monolayer discussed in Ref. 12 and shown in Fig. 1(c). We assume that the magnetic field is zero in a circular region of radius $R$ while outside this region, a constant perpendicular field is applied.

Working in polar coordinates $r$ and $\varphi$, since the vector potential of Eq. (2) preserves the circular symmetry of the problem, the $\varphi$ coordinate is cyclic and therefore one can seek the solution of Eq. (7) as $S(\mathbf{r})=S_r(r)+p_\varphi\varphi$, where $p_\varphi$ =const. Moreover, in $\varphi$ coordinate the motion is free rotation and, hence, the quantization condition for $p_\varphi$ is simply

$$\int_0^{2\pi} p_\varphi d\varphi = 2\hbar\pi m, \quad m=0,\pm 1,\pm 2\ldots, \tag{20}$$

hence, it is clear that the $p_\varphi$ quantization reads $p_\varphi=\hbar m$.

The second quantization condition can generally be written as $\frac{1}{\hbar}\oint p_r(r,m)dr+\gamma_1=2\pi(n+1/2)$ because the Maslov index is $\mu=2$ and $p_r=\frac{\partial S_r(r)}{\partial r}$. We now introduce the dimensionless variable $\xi=\frac{r^2}{2l_B^2}$ and the parameters $\delta=\frac{R^2}{2l_B^2}=\tilde{R}^2/2$ and $\tilde{m}$ $=m-\delta$. One can see that $\delta$ is basically the missing magnetic flux that can be associated with the dot. The phase accumulated between two points $\xi_1$ and $\xi_2$ inside the dot [where $B_z(r)=0$] is given by

$$S_r^{B=0}(\xi_1,\xi_2)=\frac{\hbar}{2}\int_{\xi_1}^{\xi_2} d\xi \frac{\sqrt{2\tilde{E}^2\xi-m^2}}{\xi}, \tag{21}$$

while between two points in the nonzero magnetic-field region by

$$S_r^{B\neq 0}(\xi_1,\xi_2)=\frac{\hbar}{2}\int_{\xi_1}^{\xi_2} d\xi \frac{\sqrt{-\xi^2+2(\tilde{E}^2-\tilde{m})\xi-\tilde{m}^2}}{\xi}. \tag{22}$$

[The $\hbar$ factor in the above expressions appears because in the calculation, we already took into account the quantization of $p_\varphi$, see Eq. (20).] The integrals in Eqs. (21) and (22) can be analytically calculated but the resulting expressions are too lengthy to be recorded here.

As a next step to obtain a semiclassical quantization rule, we proceed with the analysis of the classical dynamics along the lines of Ref. 31. Calculating the radial velocity $v_r(r)$ $=\frac{\hbar v_F}{E}p_r$ in the magnetic region, one finds that for $\tilde{E}^2>2\tilde{m}$ there can be two turning points in the radial motion, which we denote by $\xi_0^-$ and $\xi_0^+$. In terms of the dimensionless parameters $\tilde{R}_c=\tilde{E}$ and $\tilde{X}=\sqrt{\tilde{R}_c^2-2\tilde{m}}$ (the radius of the classical cyclotron motion and the guiding center coordinate, respectively, both in the units of $l_B$) the turning points can be written as $\xi_0^\pm=\frac{1}{2}(\tilde{R}_c\pm\tilde{X})^2$. With regard to $\delta$, there are then two possible cases:

(i) The first case is when $\delta<\xi_0^-,\xi_0^+$ (or equivalently, $\delta$ $<\frac{m^2}{2\tilde{E}^2}$) and, therefore, the radial motion is confined entirely to the magnetic region. Calculation of $\gamma_1$ gives a phase $+\pi$,

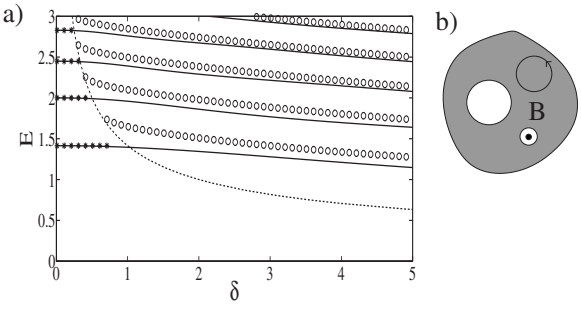


FIG. 6. (a) Results of exact quantum calculations (solid lines) for the $m=-2$ energy bands as a function of the missing flux $\delta$. The results of the semiclassical quantization (*) are obtained from Eq. (23) for $\tilde{E}<\frac{|m|}{\sqrt{2\delta}}$ and $\tilde{m}<0$. For $\tilde{E}>\frac{|m|}{\sqrt{2\delta}}$ the circles (○) show the semiclassical results calculated using Eqs. (24) and (25). The dashed line shows the $\tilde{E}=\frac{|m|}{\sqrt{2\delta}}$ function which separates the cases (i) and (ii) detailed in the main text; (b) shows a cartoon of a classical orbit in the parameter range $\tilde{E}<\frac{|m|}{\sqrt{2\delta}}$ and $\tilde{m}<0$.

which cancels the phase contribution from the Maslov index. Hence the quantization condition is $2S_r^{B\neq 0}(\xi_0^-,\xi_0^+)/\hbar=2n\pi$, where $S_r^{B\neq 0}(\xi_0^-,\xi_0^+)$ is calculated using Eq. (22). Explicitly, the energy levels $\tilde{E}_{n,m}$ are given by

$$\tilde{E}_{n,m}=\sqrt{2n+|\tilde{m}|+\tilde{m}}. \tag{23}$$

This result is very similar to what one would obtain from exact quantum calculations for a homogeneous magnetic field where the relativistic Landau levels are given by $\tilde{E}_{n,m}^{qm}$ $=\sqrt{2n+|m|+m}$. Note however that in Eq. (23) instead of the integer quantum number $m$, the noninteger $\tilde{m}=m-\delta$ appears. From Eq. (23) it is clear that for $\tilde{m}<0$ the energy bands are at $\tilde{E}_n=\sqrt{2n}$, $n=1,2,\ldots$, and they do not depend on $\delta$ and $\tilde{m}$. (As in the nanoribbon case, we exclude $n=0$ because that would give $\tilde{E}_n=0$.) These $\delta$-independent sections are readily observable in the energy bands corresponding to $m=-2$ in Fig. 6(a). On the other hand, for $\tilde{m}>0$ and $\delta\ll m$ an approxi-

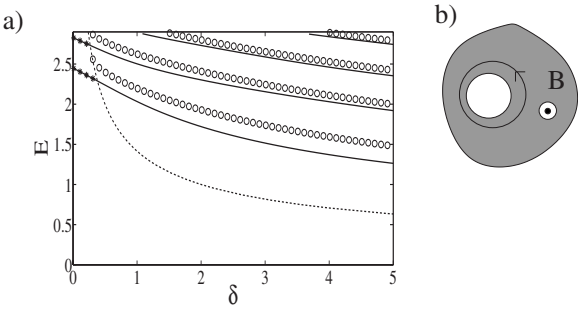


FIG. 7. (a) Results of exact quantum calculations (solid lines) for the $m=2$ energy bands as a function of the missing flux $\delta$. The results of the semiclassical quantization (*) are obtained from Eq. (23) for $\tilde{E}<\frac{|m|}{\sqrt{2\delta}}$ and $\tilde{m}>0$. For $\tilde{E}>\frac{|m|}{\sqrt{2\delta}}$ the circles (○) show the semiclassical results calculated using Eqs. (24) and (25). The dashed line shows the $\tilde{E}=\frac{|m|}{\sqrt{2\delta}}$ function which separates the cases (i) and (ii) detailed in the main text; (b) shows a cartoon of a classical orbit in the parameter range $\tilde{E}<\frac{|m|}{\sqrt{2\delta}}$ and $\tilde{m}>0$.

mately linear dependence on $\delta$ of the bands corresponding to different $m$ is predicted by Eq. (23) and this can also be observed, see Fig. 7(a). From classical point of view in the parameter range $\tilde{m}<0$ (which implies $\tilde{X}-\tilde{R}_c>\tilde{R}$), the classical orbits are such that they do not encircle the zero magnetic-field region [see Fig. 6(b)]. They are just like orbits in homogeneous magnetic field and this helps to understand why the quantum states corresponding to the same parameter range are reminiscent of dispersionless Landau levels. Conversely, for $\tilde{m}>0$ (which implies $\tilde{R}_c-\tilde{X}>\tilde{R}$) the classical orbits do encircle the zero magnetic-field region and, therefore, the energy of the corresponding quantum states depend on the missing flux $\delta$ [see the cartoon shown in Fig. 7(b) for illustration of the classical orbits].

(ii) The second case is when $\xi_0^- < \delta < \xi_0^+$, which happens if $\delta > \frac{m^2}{2\tilde{E}^2}$. The classical motion is no longer confined to the magnetic region but also enters the nonmagnetic dot. The turning point in the nonmagnetic region is at $\xi_0 = \frac{m^2}{2\tilde{E}^2} < \delta$. Since the Maslov index is $\mu=2$, the quantization condition can be written as

$$\frac{2}{\hbar}[S_r^{B=0}(\xi_0,\delta) + S_r^{B\neq 0}(\delta,\xi_0^+)] + \gamma_1 = 2\pi(n+1/2). \quad (24)$$

Here $S_r^{B=0}(\xi_0,\delta)$ and $S_r^{B\neq 0}(\delta,\xi_0^+)$ can be calculated using Eqs. (21) and (22), respectively, but the resulting expressions are again too lengthy to be presented here. Moreover, from Eq. (13) we find that

$$\gamma_1 = \frac{\pi}{2} + \arcsin\left[\frac{\tilde{E}^2 - \tilde{m} - \delta}{\sqrt{\tilde{E}^2(\tilde{E}^2 - 2\tilde{m})}}\right]. \quad (25)$$

One can see that here in general, $\gamma_1 \neq \pi$ and, therefore, it does not cancel the contribution of the Maslov index.

As one can observe the overall agreement of the exact quantum and of the semiclassical calculations shown in Figs. 6 and 7 is good, especially for higher energies. According to the exact quantum calculations,[12] there is also a zero-energy state but this cannot be described by our semiclassics.

## VI. CONCLUSIONS

To conclude, using semiclassical quantization we have studied the spectrum of bound states in inhomogeneous magnetic-field setups in graphene monolayer and bilayer. We have found that a semiclassical quantization, which takes into account a Berry-like phase, can indeed explain all the main features of the exact quantum or numerical TB calculation. In particular, we have studied graphene monolayer and bilayer nanoribbons in magnetic waveguide configuration and also in a configuration when snake states can exist. Besides, we have discussed the magnetic dot system in graphene monolayer. For the considered stepwise constant magnetic-field profile, we have derived semiclassical quantization equations. In the case of graphene monolayer, we have compared the resulting semiclassical eigenenergies with quantum-mechanical ones obtained from the corresponding Dirac equation. For graphene bilayer the results of the semiclassical quantization and numerical TB calculations have been compared. In all the cases a good agreement has been found except for energies very close to the Dirac point. We have shown that the main features of the spectrum depend on whether the classical guiding center coordinate is in the nonmagnetic or in the magnetic-field region.

Assuming homogeneous magnetic field, the energy of the Landau levels in semiclassical approximation was calculated in Ref. 20. Our work can be considered as a generalization of these calculations to a class of nonhomogeneous magnetic-field setups, where due to the symmetry of the system, the Berry-like phase appearing in the semiclassical theory affects only one of the quantization conditions.

## ACKNOWLEDGMENTS

We acknowledge the discussions with Henning Schomerus. This work was supported partly by the European Commission under Contract No. MRTN-CT-2003–504574 and by EPSRC. J.Cs. would like to acknowledge the support of the Hungarian Science Foundation OTKA under Contract No. T48782.

[1] K. S. Novoselov, A. K. Geim, S. V. Morozov, D. Jiang, Y. Zhang, S. V. Dubonos, I. V. Grigorieva, and A. A. Firsov, Science **306**, 666 (2004); K. S. Novoselov, A. K. Geim, S. V. Morozov, D. Jiang, M. I. Katsnelson, I. V. Grigorieva, S. V. Dubonos, and A. A. Firsov, Nature (London) **438**, 197 (2005).

[2] Y. Zhang, J. P. Small, M. E. S. Amori, and P. Kim, Phys. Rev. Lett. **94**, 176803 (2005); Y. Zhang, Y.-W. Tan, H. L. Stormer, and P. Kim, Nature (London) **438**, 201 (2005).

[3] K. S. Novoselov, E. McCann, S. V. Morozov, V. I. Fal'ko, M. I. Katsnelson, U. Zeitler, D. Jiang, F. Schedin, and A. K. Geim, Nat. Phys. **2**, 177 (2006).

[4] M. I. Katsnelson, Mater. Today **10**, 20 (2007).

[5] M. I. Katsnelson and K. S. Novoselov, Solid State Commun. **143**, 3 (2007).

[6] A. K. Geim and K. S. Novoselov, Nat. Mater. **6**, 183 (2007).

[7] A. H. Castro Neto, F. Guinea, N. M. R. Peres, K. S. Novoselov, and A. K. Geim, arXiv:0709.1163, Rev. Mod. Phys. (to be published).

[8] Johan Nilsson, A. H. Castro Neto, F. Guinea, and N. M. R. Peres, Phys. Rev. B **78**, 045405 (2008).

[9] Solid State Commun. **143**, 1 (2007), special issue on graphene.

[10] Besides the review articles (Refs. 4–8), see, e.g., Y. Zheng and T. Ando, Phys. Rev. B **65**, 245420 (2002); V. P. Gusynin and S. G. Sharapov, Phys. Rev. Lett. **95**, 146801 (2005); Phys. Rev. B **73**, 245411 (2006); M. Tahir and K. Sabeeh, *ibid.* **76**, 195416 (2007).

[11] E. McCann and V. I. Fal'ko, Phys. Rev. Lett. **96**, 086805 (2006).

[12] A. De Martino, L. Dell'Anna, and R. Egger, Phys. Rev. Lett. **98**, 066802 (2007).

[13] J. E. Müller, Phys. Rev. Lett. **68**, 385 (1992).

[14] J. Reijniers and F. M. Peeters, J. Phys.: Condens. Matter **12**, 9771 (2000); J. Reijniers, A. Matulis, K. Chang, F. M. Peeters, and P. Vasilopoulos, Europhys. Lett. **59**, 749 (2002); H. Xu, T. Heinzel, M. Evaldsson, S. Ihnatsenka, and I. V. Zozoulenko, Phys. Rev. B **75**, 205301 (2007).
[15] L. Oroszlány, P. Rakyta, A. Kormányos, C. J. Lambert, and J. Cserti, Phys. Rev. B **77**, 081403(R) (2008).
[16] T. K. Ghosh, A. De Martino, W. Häusler, L. Dell'Anna, and R. Egger, Phys. Rev. B **77**, 081404(R) (2008).
[17] N. Nemec and G. Cuniberti, Phys. Rev. B **74**, 165411 (2006).
[18] H. W. Lee and D. S. Novikov, Phys. Rev. B **68**, 155402 (2003).
[19] M. Ramezani Masir, P. Vasilopoulos, A. Matulis, and F. M. Peeters, Phys. Rev. B **77**, 235443 (2008).
[20] Pierre Carmier and Denis Ullmo, Phys. Rev. B **77**, 245413 (2008).
[21] K. Yabana and H. Horiuchi, Prog. Theor. Phys. **75**, 592 (1986); **77**, 517 (1987).
[22] R. G. Littlejohn and W. G. Flynn, Phys. Rev. A **44**, 5239 (1991).
[23] K. P. Duncan and B. L. Györffy, Ann. Phys. (N.Y.) **298**, 273 (2002).
[24] S. Keppeler, Ann. Phys. (N.Y.) **304**, 40 (2003).
[25] K. Wakabayashi, M. Fujita, H. Ajiki, and M. Sigrist, Phys. Rev. B **59**, 8271 (1999).
[26] M. Brack and R. K. Bhaduri, *Semiclassical Physics*, Frontiers in Physics Vol. 96 (Addison-Wesley, Reading, MA, 1997).
[27] T. Ohta, A. Bostwick, T. Seyller, K. Horn, and E. Rotenberg, Science **313**, 951 (2006).
[28] Generally, by using group theoretical arguments one can show that if the system has a continuous symmetry, described by a one-parameter symmetry transformation $\hat{S}(\theta)$, then from Eq. (10) it follows that $\gamma(\mathbf{r})$ can only depend on the fundamental invariant $F(\mathbf{r})$ of $\hat{S}(\theta)$. Here $F(\mathbf{r})$ is a particular function of the coordinates and together with an appropriately chosen $G(\mathbf{r})$ function, they can define a new (curvilinear) coordinate system. In this new coordinate system then our considerations leading to Eq. (13) do apply. For the graphene monolayer examples, where the exact quantum solutions of the problems are known, this can also be verified by taking the short-wavelength asymptotic form of the quantum wave functions.
[29] For the magnetic field used in our TB calculations the sequence of the Landau levels in bilayer is given by $E_n \hbar \omega_c \sqrt{n(n-1)}$ (see Ref. 11). Therefore the $n=0$ and 1 levels are degenerate and another twofold degeneracy comes from the electron-hole symmetry of the Hamiltonian.
[30] Tight-binding (TB) calculations for a bilayer graphene system in homogeneous perpendicular magnetic field have been published in, e.g., Eduardo V. Castro, N. M. R. Peres, and J. M. B. Lopes dos Santos, Phys. Status Solidi B **244**, 2311 (2007). However, to our best knowledge TB or analytic calculations for the magnetic field profile shown in Figs. 1(a) and 1(b) have not yet been published. In the numerical calculations presented in Sec. IV the width of the graphene ribbon was $L=(\sqrt{3}N-1)a$ where $N=2400$ is the number of lattice sites in the $x$ direction. Furthermore, we used $t_2/t_1=0.156$ and the strength of the magnetic field was 1 T.
[31] B. Kocsis, G. Palla, and J. Cserti, Phys. Rev. B **71**, 075331 (2005).